ACS APPLIED MATERIALS & INTERFACES

Research Article

www.acsami.org

In Situ Precipitation of Te Nanoparticles in p-Type BiSbTe and the Effect on Thermoelectric Performance

Ting Zhang, Jun Jiang,* Yukun Xiao, Yongbiao Zhai, Shenghui Yang, and Gaojie Xu

Ningbo Institute of Materials Technology and Engineering, Chinese Academy of Sciences, Ningbo 315201, China

ABSTRACT: Through zone melting method, a certain amount of Te nano precipitations were in situ generated in the p-type BiSbTe matrix because of the addition of graphene. Both the microstructure and thermoelectric performance were investigated. Increased carrier concentration was obtained to improve the electrical performance, and the lattice thermal conductivity was simultaneously lowered about 25% by Te nano precipitations as phonon scattering centers. Consequently, an optimization of the thermoelectric figure-of-merit ZT between 375 and 550 K was achieved.

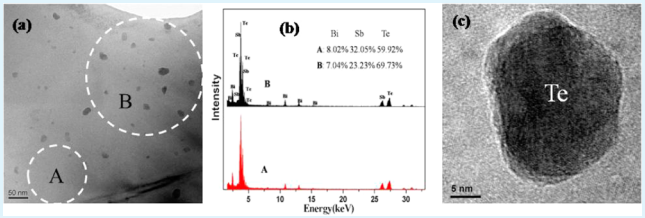

KEYWORDS: *p-type BiSbTe, graphene, Te nanoparticles, In Situ precipitation, thermoelectric performance, zone melting*

1. INTRODUCTION

Bi_2Te_3-based alloys are one of the most excellent thermoelectric (TE) materials near room temperature, which can be used as power generation or device cooling by directly conversion between heat and electricity with no moving parts or environmentally harmful fluids.[1−3] The conversion efficiency depends on the dimensionless TE figure of merit $ZT = \alpha^2\sigma T/\kappa = \alpha^2\sigma T/(\kappa_L + \kappa_e)$, where α is the Seebeck coefficient, σ the electrical conductivity, κ the thermal conductivity (including the lattice κ_L and carrier κ_e contributions), and T is the absolute temperature.[4,5]

To date, ZT value of the traditional Bi_2Te_3-based alloys remains about 1.0. However, higher ZT values have been achieved in experimental studies by introducing nanostructure to reduce the lattice thermal conductivity. For example, Venkatasubramanian et al.[6] produced a layered Bi_2Te_3/Sb_2Te_3 superlattice with a ZT of 2.4, Ren et al.[7] obtained a ZT of 1.4 for the nanostructured bulk BiSbTe by ball-milling and hot-pressing, and Tang et al.[8] reported the melt-spun BiSbTe alloys with a ZT of 1.56.

Many methods can be used to produce nanostructured TE materials. Besides sintering nanoparticles into solid[9−12] or embedding nanoparticles in the matrix,[13−16] in situ generation of nano precipitations as a second phase is also an effective method, which can naturally form nanostructure and avoid complicated post-treatment.[16] Kanatzidis's group has done a lot of work about in situ generation of nanostructured phase by spinodal decomposition or solid solution in PbTe-based TE materials, such as PbTe-PbS 8%,[17] $AgPb_mSbTe_{2+m}$,[18] $Pb_{1-x}Sn_xTe$-PbS,[19] and $Na_{1-x}Pb_mSb_yTe_{m+2}$,[20] all of which have obtained excellent TE performance. However, for Bi_2Te_3-based alloys, it is a little rare and difficult to in situ generate nanophase by the above methods. In the present study, we report a new way to achieve in situ generation of nano phase in the zone melted p-type BiSbTe ingot by adding graphene. Since graphene is one kind of material with many special characterizations, such as the layered structure, high electrical conductivity, and graphene also possesses the similar chemical properties with graphite,[21−23] we hope to investigate the effect of graphene on the TE performance of the layered Bi_2Te_3-based materials. We find a certain amount of Te nano precipitations have been in situ generated in the BiSbTe matrix and thus affected the TE performance.

2. EXPERIMENTAL SECTION

2.1. Materials and Methods. Elements of Bi, Sb, Te (Alfa Aesar, 99.99%) with size of about 120−180 μm were employed as precursors, and graphene powder with size of about 200 nm and surface area of at least 300 m^2/g was added into the matrix elements. All of the chemicals were used without further purification. Thus the p-type BiSbTe alloy with Te nano precipitations was prepared using zone melting method by adding graphene powder. To analyze the effect of graphene powder on the TE performance, we also prepared pure BiSbTe in the same condition.

2.2. Synthesis of the Samples. Stoichiometric amounts of Bi, Sb, Te (Alfa Aesar, 99.99%) to synthesis $Bi_{0.5}Sb_{1.5}Te_3$ were weighted and charged into a quartz tube, respectively with x wt % (x = 0 and 0.09) graphene powder. The quartz tubes were evacuated, sealed, and then melted at 973 K for 2 h using a rocking furnace to ensure composition homogeneity. After quenching to room temperature, the crystals were grown in a zone melting furnace at a temperature of 1023 K with a growth speed of 25 mm/h. It is worthy to note that most of the graphene powder has been removed to the top of ingot during the zone melting process due to its extremely low density. Bars of 2 mm × 2 mm × 10 mm and plates of Φ 10 mm × 2.0 mm were cut from the ingots along growth direction to measure the transport properties.

2.3. Instruments and Characterization. The phase structure of the prepared samples were characterized by X-ray powder diffraction (XRD) using Cu Kα radiation (λ = 1.5406 Å). The microstructure was investigated using scanning electron microscopy (FESEM, Hitachi S4800) and transmission electron microscopy (TEM, Tecnai F20,

Received: December 28, 2012
Accepted: April 1, 2013
Published: April 1, 2013

FEI) with energy dispersive spectrometry (EDS). The electrical conductivity (σ) and Seebeck coefficient (α) were measured simultaneously on bars of 2 mm × 2 mm × 10 mm using ZEM-3 system (ULVAC Co., Ltd.) in the temperature range of 300−550 K. The carrier concentration (p) and mobility (μ) were calculated from the Hall coefficient (R_H) measured by a physical properties measurement system (Quantum Design, PPMS-9). The thermal conductivity (κ) was calculated from the values of thermal diffusivity (λ), density (ρ), and specific heat (C_p) by the relationship $\kappa = \lambda\rho C_p$, in which λ was measured using a laser flash system (Netzsch LFA-457) and C_p was measured by a differential scanning calorimeter (Shimadzu DSC-50) under an Ar flow on the plates of Φ 10 mm × 2.0 mm.

3. RESULTS AND DISCUSSION

3.1. Phase Structure. Figure 1 shows the XRD patterns of the prepared samples. We designate the sample of BiSbTe doped with 0.09 wt % graphene as BiSbTe+G and pure BiSbTe as BiSbTe. It can be seen that both BiSbTe and BiSbTe+G possess the main phase of BiSbTe structure with space group $R\bar{3}m$. Moreover, some obvious supernumerary peaks corresponding to Te have emerged as marked in the pattern of BiSbTe+G, implying that a second phase of Te was generated.

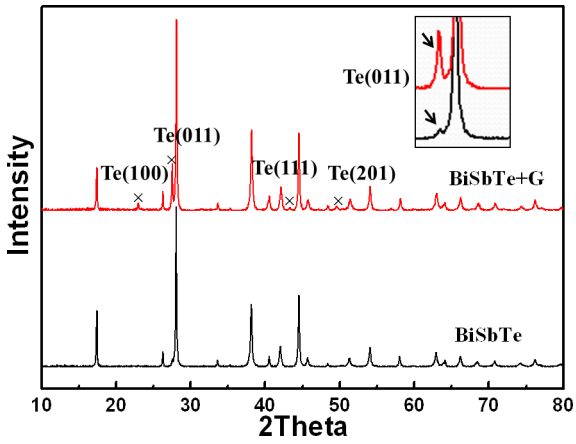

Figure 1. XRD patterns of BiSbTe+G and BiSbTe with the enlarged Te (0 1 1) peak (inset).

In fact, certain Te phase usually can be found in the BiSbTe alloy because some extra Te element is added in the matrix composition, as shown in the enlarged Te (0 1 1) peak. However, under the same conditions of matrix composition and preparation, the amount of second Te phase in BiSbTe+G sample is much more than that in BiSbTe. We speculate the possible reason is related to the addition of graphene. As we know, graphene is one kind of material with many special characterizations, such as the layered structure and high electrical conductivity, and graphene also possesses chemical properties similar to that of graphite.[21−23] We consider that the precipitation of the Te phase is related to the oxidative performance of graphene, which can accept electrons and react with some molten Bi or Sb atoms at high temperature, causing more extra Te element was generated as a second phase.

3.2. Microstructure. The SEM and TEM images of BiSbTe +G are listed in Figure 2 and Figure 3. Both the planes perpendicular and parallel to the zone melting direction in Figure 2 show that a certain amount of grains precipitate in the matrix. Besides, we also find some layered graphene still remain in the matrix as shown in images a and b in Figure 2.

Figure 3 shows the TEM images of sample BiSbTe+G. In Figure 3a, it can be observed that the generated precipitations are in size of about 10−30 nm dispersed in the matrix, which can play as scattering centers and have the effect of depressing κ_L over a wide scare. From the corresponding EDS analysis (Figure 3b), we can see that the area B with nano precipitations is rich in Te element compared to the matrix area A, which can further confirm the precipitate of the nanosized Te phase. In Figure 3c, the HRTEM (high-resolution transmission electron microscopy) image shows a typical second phase of the nanoscaled Te precipitation with about 20 nm coherently locates in the BiSbTe matrix.

3.3. Thermoelectric Performance. Effects of the Te precipitations on the thermoelectric performance are displayed in Figure 4. It can be observed in Figure 4a that the electrical conductivities decrease with increasing temperature from 300 to 550 K for both samples, showing metallic electrical properties. Over the whole temperature range, the BiSbTe+G sample possesses a higher σ than that of BiSbTe. Especially at 300 K, the σ value is significantly enhanced from 1.83×10^5 S/m to 3.02×10^5 S/m. This increased σ mainly comes from the enhancement of carrier concentration p from 1.9×10^{19} cm^{-3} to 4.7×10^{19} cm^{-3} (inset of Figure 4a), which is calculated from the Hall coefficient measured at 300 K. Te precipitated and the composition of matrix was changed when added graphene, which may result in the variation of carrier concentration. However, the influence factors are complicated and needed to be further investigated. On the other hand, the carrier mobility

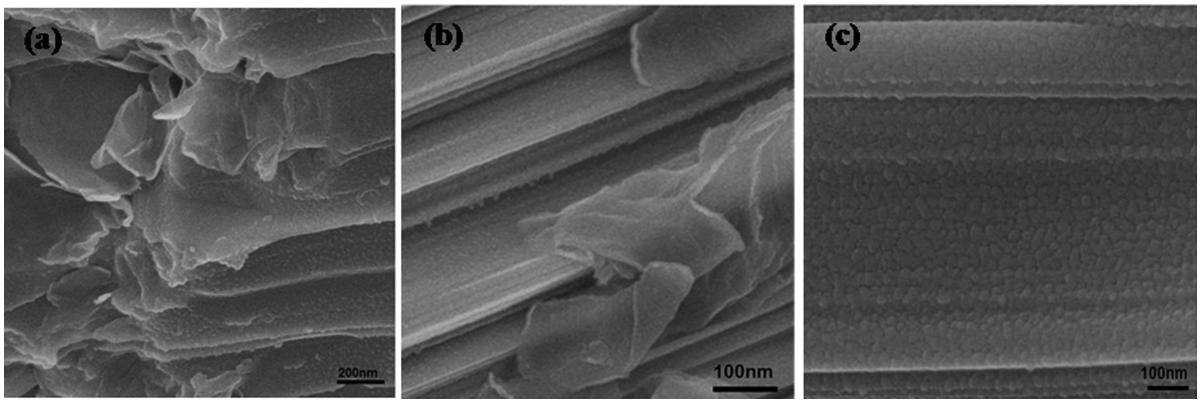

Figure 2. SEM images of the planes (a, b) perpendicular and (c) parallel to zone melting direction for BiSbTe+G, showing nano precipitations are generated in the matrix.

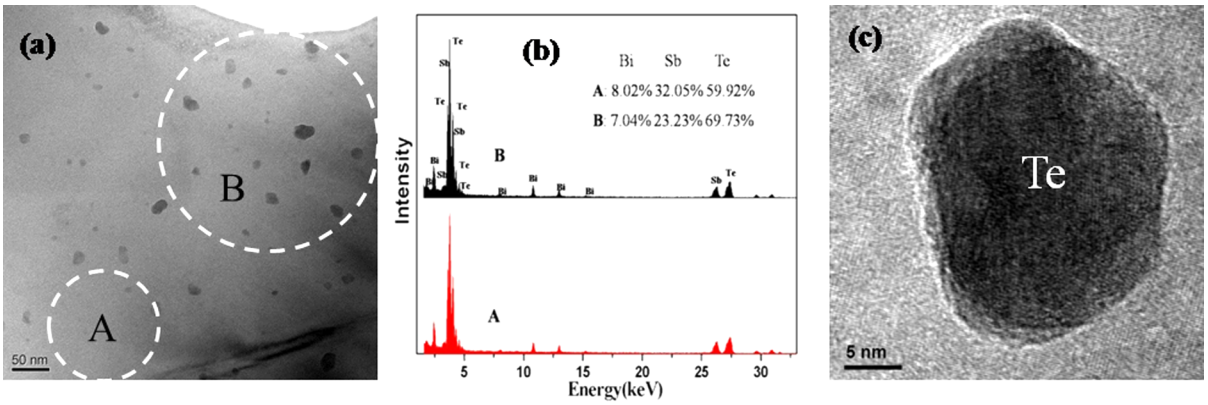

Figure 3. (a) TEM and (c) HRTEM images for BiSbTe+G. (b) The corresponding EDS results for the areas A and B marked in a.

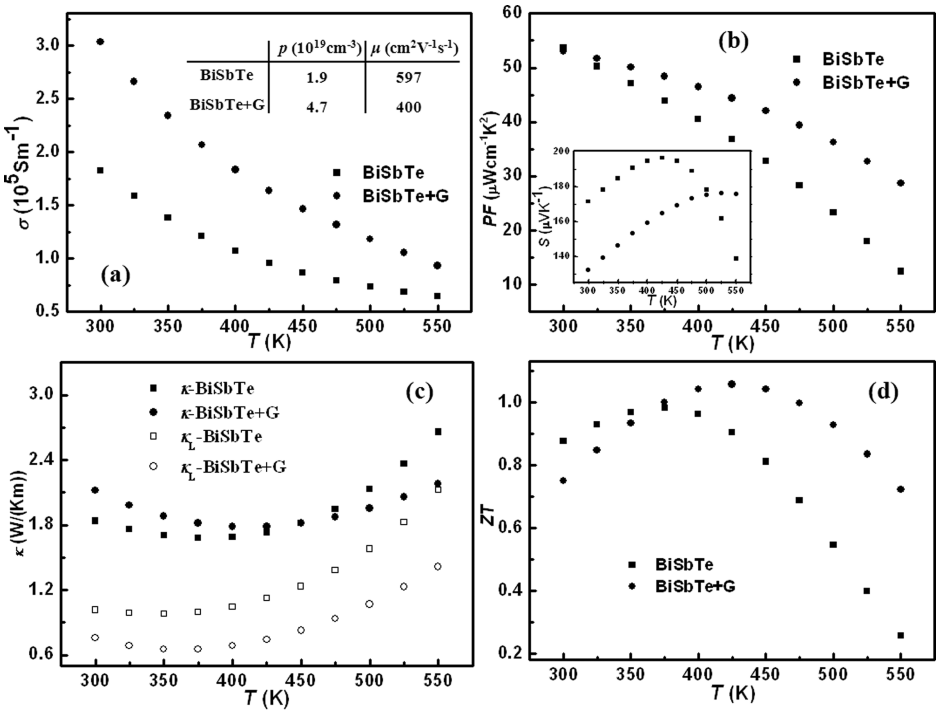

Figure 4. Temperature Dependence of TE performance for BiSbTe and BiSbTe+G: (a) electrical conductivity σ (inset: carrier concentration p and mobility μ at 300 K); (b) power factor $PF = \alpha^2\sigma$ (inset: Seebeck coefficient α); (c) thermal conductivity κ and lattice thermal conductivity κ_L; (d) ZT.

μ has declined from 597 $cm^2\ V^{-1}\ s^{-1}$ to 400 $cm^2\ V^{-1}\ s^{-1}$ at 300 K, which can be mainly ascribed to the blocking of the carrier transport by the nanosized Te precipitations.

The inset of Figure 4b shows the Seebeck coefficient α for BiSbTe+G is much lower than that of BiSbTe below 500 K, which is mainly due to the increased p in BiSbTe+G. Furthermore, the peak value of α, resulting from the intrinsic excitation, has been restrained toward higher temperature by the increased p of BiSbTe+G, from 425 to 525 K. It is similar with description in ref 24. As a result, the calculated PF values are very close for BiSbTe and BiSbTe+G at 300 K, but much higher for BiSbTe+G than BiSbTe with increasing temperature (Figure 4b).

The temperature dependence of thermal conductivity κ and lattice thermal conductivity κ_L is displayed in Figure 4c. Here, the κ_L can be calculated by: $\kappa_L = \kappa - \kappa_e = \kappa - L\sigma T$, where κ_e is the electronic thermal conductivity, L is the Lorenz number, about $1.5 \times 10^{-8}\ V^2\ K^{-2}$,which is obtained from fitting the Seebeck data to the reduced chemical potential.[25] For BiSbTe +G, the κ_L is about 25% lower than that of BiSbTe. The significant depression of κ_L can be ascribed to the effective scattering of the generated Te phase and the residual graphene in the matrix as mentioned above. However, the κ for BiSbTe +G is a little higher than that of BiSbTe below 450 K, mainly because of its higher electronic thermal conductivity.

As a result, the figure-of-merit ZT (Figure 4d) between 375 and 550 K for BiSbTe+G has been optimized compared to BiSbTe, and a maximum ZT for BiSbTe+G of 1.05 was obtained at 425 K. In fact, the precipitation of Te nanoparticles has not only significantly reduced the κ_L but also increased the carrier concentration, thus resulting in a high κ. To get a relatively lower thermal conductivity and higher ZT, further experimental processes of tuning carrier concentration, such as doping, but not influencing the nano precipitations is needed.

dx.doi.org/10.1021/am303145v | ACS Appl. Mater. Interfaces 2013, 5, 3071−3074

4. CONCLUSIONS AND SUMMARIES

In summary, the in situ precipitations are obtained in Bi_2Te_3-based alloys by adding graphene powder through zone melting method. The electrical performance has been improved mainly due to the increased carrier concentration. The nanosized Te precipitations have resulted in more scattering of phonons and significantly reduced the lattice thermal conductivity. Finally, an optimization of figure-of-merit *ZT* between 375 and 550 K has been achieved.

AUTHOR INFORMATION

Corresponding Author

*Tel.: +86 574 87913381. Fax: +86 574 86685163. E-mail: jjun@nimte.ac.cn.

Notes

The authors declare no competing financial interest.

ACKNOWLEDGMENTS

This work was partially supported by the NSFC (51201175), Zhejiang Provincial Public Welfare Technology Program (2010C31106, 2012C21109), the Science Foundation of Ningbo (2011A610096), and the aided program for Science and Technology Innovative Research Team of Zhejiang Province and Ningbo Municipality (2009B21005).

REFERENCES

(1) Bell, L. E. *Sci.* **2008**, *321*, 1457.
(2) Tritt, T. M. *Annu. Rev. Mater. Res.* **2011**, *41*, 433.
(3) Pei, Y. Z.; Shi, X. Y.; Lalonde, A.; Wang, H.; Chen, L. D.; Snyder, G. J. *Nature* **2011**, *473*, 66.
(4) Ioffe, A. F., *Semiconductor Thermoelements, and Thermoelectric Cooling*; Infosearch: London, 1957.
(5) Snyder, G. J.; Toberer, E. S. *Nat. Mater.* **2008**, *7*, 105.
(6) Venkatasubramanian, R.; Siivola, E.; Colpitts, T.; O'Quinn, B. *Nature* **2001**, *413*, 597.
(7) Poudel, B.; Hao, Q.; Ma, Y.; Lan, Y. C.; Minnich, A.; Yu, B.; Yan, X.; Wang, D. Z.; Muto, A.; Vashaee, D.; Chen, X. Y.; Liu, J. M.; Dresselhaus, M. S.; Chen, G.; Ren, Z. F. *Sci.* **2008**, *320*, 634.
(8) Xie, W. J.; Tang, X. F.; Yan, Y. G.; Zhang, Q. J.; Tritt, T. M. *Appl. Phys. Lett.* **2009**, *94*, 102111.
(9) Gothard, N.; Ji, X.; He, J.; Tritt, T. M. *J. Appl. Phys.* **2008**, *103*, 054314.
(10) Ma, Y.; Hao, Q.; Poudel, B.; Lan, Y. C.; Yu, B.; Wang, D. Z.; Chen, G.; Ren, Z. F. *Nano Lett.* **2008**, *8*, 2580.
(11) Tang, X. F.; Xie, W. J.; Li, H.; Zhao, W. Y.; Zhang, Q. J. *Appl. Phys. Lett.* **2007**, *90*, 012102.
(12) Cao, Y. Q.; Zhao, X. B.; Zhu, T. J.; Zhang, X. B.; Tu, J. P. *Appl. Phys. Lett.* **2008**, *92*, 143106.
(13) Zhao, L. D.; Zhang, B. P.; Li, J. F.; Zhou, M.; Liu, W. S.; Liu, J. *J. Alloys Compd.* **2008**, *455*, 259.
(14) Zhang, T.; Zhang, Q. S.; Jiang, J.; Xiong, Z.; Chen, J. M.; Zhang, Y. L.; Li, W.; Xu, G. J. *Appl. Phys. Lett.* **2011**, *98*, 022104.
(15) Xiong, Z.; Chen, X. H.; Zhao, X. Y.; Bai, S. Q.; Huang, X. Y.; Chen, L. D. *Solid State Sci.* **2009**, *11*, 1612.
(16) Zhang, B.; Sun, J.; Katz, H. E.; Fang, F.; Opila, R. L. *ACS Appl. Mater. Inter.* **2010**, *2*, 3170.
(17) Girard, S. N.; He, J. Q.; Li, C. P.; Moses, S.; Wang, G. Y.; Uher, C.; Dravid, V. P.; Kanatzidis, M. G. *Nano Lett.* **2010**, *10*, 2826.
(18) Hsu, K. F.; Loo, S.; Guo, F.; Chen, W.; Dyck, J. S.; Uher, C.; Hogan, T.; Polychroniadis, E. K.; Kanatzidis, M. G. *Sci.* **2004**, *303*, 818.
(19) Androulakis, J.; Lin, C. H.; Kong, H. J.; Uher, C.; Wu, C. L.; Hogan, T.; Cook, B. A.; Caillat, T.; Paraskevopoulos, K. M.; Kanatzidis, M. G. *J. Am. Chem. Soc.* **2007**, *129*, 9780.
(20) Poudeu, P. F. P.; D'Angelo, J.; Downey, A. D.; Short, J. L.; Hogan, T. P.; Kanatzidis, M. G. *Angew. Chem.* **2006**, *118*, 3919.
(21) Geim, A. K.; Novoselov, K. S. *Nat. Mater.* **2007**, *6*, 183.
(22) Balandin, A. A.; Ghosh, S.; Bao, W.; Calizo, I.; Teweldebrhan, D.; Miao, F.; Lau, C. N. *Nano Lett.* **2008**, *8*, 902.
(23) Fu, Q.; Bao, X. H. *Chin. Sci. Bull.* **2009**, *54*, 2657.
(24) Zhang, T.; Jiang, J.; Xiao, Y. K.; Zhai, Y. B.; Yang, S. H.; Xu, G. J. *J. Mater. Chem. A* **2013**, *1*, 967.
(25) Biswas, K.; He, J. Q.; Blum, I. D.; Wu, C.; Hogan, T. P.; Seidman, D. N.; Dravid, V. P.; Kanatzidis, M. G. *Nature* **2012**, *489*, 416.